Saudi Pharmaceutical Journal 31 (2023) 669–677

HOSTED BY

Contents lists available at ScienceDirect

Saudi Pharmaceutical Journal

journal homepage: www.sciencedirect.com

Original article

Formulation and characterization of thiolated chitosan/polyvinyl acetate based microneedle patch for transdermal delivery of dydrogesterone

Amna Khalid [a], Hafiz Shoaib Sarwar [b,*], Muhammad Sarfraz [c], Muhammad Farhan Sohail [a], Aamir Jalil [f], Yousef A. Bin Jardan [d], Rabia Arshad [e], Ifrah Tahir [g], Zulcaif Ahmad [e]

[a] Riphah Institute of Pharmaceutical Sciences Riphah International University, Lahore, Campus, Pakistan
[b] Faculty of Pharmaceutical Sciences, University of Central Punjab, Lahore, Pakistan
[c] College of Pharmacy, Al Ain University, Al Ain, United Arab Emirates
[d] Department of Pharmaceutics, College of Pharmacy, King Saaud University, Riyadh, Saudi Arabia
[e] Faculty of Pharmacy, University of Lahore, Lahore, Pakistan
[f] Faculty of Pharmacy, Bahuddin Zakariya University, Multan, Pakistan
[g] Forman Christian College, Lahore, Pakistan

ARTICLE INFO

Article history:
Received 7 December 2022
Accepted 8 March 2023
Available online 15 March 2023

Keywords:
Microneedle patches
Thiolated chitosan
Transdermal delivery
Dydrogesterone

ABSTRACT

Microneedle patches are promising transdermal drug delivery platforms with minimal invasiveness in a painless manner. Microneedle patch could be a promising alternate route for delivery of drugs having poor solubility and low bioavailability. This research work therefore, aimed to develop and characterize microneedle patch of thiolated chitosan (TCS) and polyvinyl acetate (PVA) for the systemic delivery of dydrogesterone (DYD). TCS-PVA-based microneedle patch was fabricated with 225 needles having a length of 575 µm with the sharp pointed end. Different ratios of TCS-PVA-based patch were employed to investigate the effects of mechanical tensile strength and percentage elongation. The scanning electron microscopy (SEM) revealed intact sharp-pointed needles. *In vitro* dissolution studies of microneedle patch (MN-P) were carried out by modified Franz-diffusion cell revealing the sustained release of DYD 81.45 ± 2.768 % at 48 hrs as compared to pure drug that showed 96.7 ± 1.75 % at 12 hrs. The transport of DYD (81%) across skin reaching the systemic circulation was evaluated through *ex vivo* permeation studies of MN-P. The skin penetration study through the parafilm M method showed good penetration with no deformation and breakage of needles along with no visible signs of skin irritation. Histological study of mice skins clearly showed the deeper penetration of needles into the skin. In summary, as-prepared MN-P show potential in developing an effective transdermal delivery system for DYD.

1. Introduction

The skin offers an available and appropriate site for the administration of biomedicines (Arshad et al., 2019). To this end, the field of transdermal drug delivery system (TDDS), has emerged as a safe and effective means of delivering medications across the skin (Sabbagh and Kim 2022). TDDS-based therapy is cost-effective as it aids in preventing polypharmacy and has increased the patient's compliance *by* simplifying the application procedure (Sabbagh and Kim 2022). Moreover, before conventional oral and parenteral route-based dosage forms, there is an urge for eco-friendly technology that can effectively deliver therapeutic amounts of the drug(s) at the site of action (Jung and Jin 2021, Sabbagh and Kim 2022).

Microneedles technology has revolutionized the field of TDDS as an alternative to conventional oral and parenteral dosage forms for the painless delivery of biomedicines across the skin (Sabo and Waters 2021). Microneedle patches (MN-P) can deviate in terms of various constructed features like the aspect of length, tip diameter, base diameter, needle-to-needle spacing, and array dimensions (Elahpour et al., 2021). Dydrogesterone (DYD) is a synthetic pro-

* Corresponding author.
E-mail addresses: Shoaib.sarwar@ucp.edu.pk (H. Shoaib Sarwar), muhammad.sarfraz@aau.ac.ae (M. Sarfraz), farmacist.pk@gmail.com (M. Farhan Sohail), aamirs.jalil@gmail.com (A. Jalil), Ybinjardan@ksu.edu.sa (Y.A. Bin Jardan), rabia.arshad@pharm.uol.edu.pk (R. Arshad), zulcaifa@gmail.com (Z. Ahmad).
Peer review under responsibility of King Saud University.

Production and hosting by Elsevier

https://doi.org/10.1016/j.jsps.2023.03.007
1319-0164/

gesterone analogue being widely used in the therapy of several gynaecological disorders (Amer et al., 2021). However, oral DYD intake is accompanied with poor bioavailability owing to minimal water solubility and extensive hepatic first-pass metabolism (Sharma et al., 2021). The decreased oral bioavailability along with longer duration hormone replacement therapy creates the needs for the transdermal delivery of the hormones and synthetic analogues. Therefore, DYD can be a suitable candidate transdermal delivery, especially via microneedle patches owing to its large molecular structure.

The microneedle patches can be designed with various polymeric excipients to impart discrete properties to the patches like the dissolution of microneedles, crosslinked matrix to limit dissolution of needles, enhancement of the mechanical properties etc. Thiolated chitosan is one the Widley explored polymeric excipient for its thiomeric profile owing to the covalent attachment of the thiol groups. These properties include, permeation enhancement, mucoadhesion and disulfide bond formation. This study reports the use of thiolated chitosan because of its ability to developed disulfide bonds leading to the crosslinked matrix providing strength to the microneedles. Another useful polymer, being exploited in the current work is polyvinyl acetate commonly (PVA). However, PVA is a hydrophilic synthetic polymer, being featured with mechanical strength, flexibility, biocompatibility and stability (Parın et al., 2022).

Therefore, this study was aimed to developed disulfide crosslinked TCS/ PVA based transdermal patches loaded with DYD for the prolonged delivery via transdermal route.

2. Materials

Chitosan (LMW with degree of deacetylation of 75–85%) was obtained from BDH, England. Dydrogesterone was received as a gift from Highnoon Laboratories Ltd, Pakistan. Polyvinyl acetate, Thioglycolic Acid (99%), 1-Ethyl-3-(3-dimethylaminopropyl)carbodii mide (EDAC) and Ellman's reagent (5,5-dithiobis (2-nitro benzoic acid were obtained from Sigma- Aldrich, Germany. Polydimethylsiloxane (PDMS) molds were purchased from Micro point Technology, Singapore.

3. Methods

3.1. Synthesis of thiolated chitosan

To prepare 1% solution of chitosan, chitosan was hydrated in 1% acetic acid by stirring overnight followed by the addition of 1 ml of thioglycolic acid (TGA). Then 125 mM 1-ethyl-3-(3-dimethylaminopropyl) carbodiimide (EDAC) was added to activate the carboxyl group of TGA. The pH of the reaction mixture was adjusted to 5 using 1 M NaOH solution and stirring was continued for 4 h. The mixture was dialyzed by using a cellulose membrane (molecular weight cut-off 12–14 kDa) five times for 3 days and kept under dark conditions at room temperature. The polymeric mixture was dialyzed for one time with 5 mM HCl solution continued for the next two times with 5 mM HCl with the addition of 1% NaCl to quench ionic interaction between anionic sulfhydryl group and cationic polymer. The last two times were dialyzed with 1 mM HCl solution to maintain the pH at 4.0. The final purified TCS was lyophilized using a lyophilizer (Scanvac cool safe 110–4) and kept at 4 °C until the further use (Iqbal et al., 2012).

3.2. Determination of thiol content

The amount of thiol group in TCS conjugates was determined *via* spectrophotometry by reaction with *Ellman's* reagent (3 mg in 10 ml of 0.5 M phosphate buffer). 0.5 mg of TCS was dissolved in 250 µl deionized water, 250 µl of 0.5 M phosphate buffer (pH 8.0) then 500 µl Ellman's reagent was added. The samples were incubated at room temperature, undisturbed for 3 h in dark. Thereafter, absorbance was measured at a wavelength of 430 nm of the supernatant obtained after centrifugation. TGA standards were used to determine the number of thiol moieties on the chitosan polymer (Saremi et al., 2011).

3.3. Determination of disulfide bonds

TCS conjugates were hydrated in 350 µl of deionized water, then 650 µl of 0.05 M phosphate buffer (pH-6.8) was added. After 30 min, 1 ml of 4% sodium borohydride solution and 200 µl of 5 M HCl added to the sample solution. This sample solution was incubated for 1 h at 37 °C followed by 1 ml of 1 M phosphate buffer (pH-8.5) with the addition of 100 µl of Ellman's reagent. After an hour of incubation, a sample of 300 µl was transferred to a microwell plate and absorbance was measured via plate reader at 430 nm (PerkinElmer, USA). The remaining thiol group amount was evaluated by deduction of thiol group from total thiol content fixed on polymer (Bernkop-Schnürch et al., 1999).

3.4. Development of MNP- and PVA-based microneedle patch

Microneedle patch (MN-P) of TCS and polyvinyl acetate (PVA) loaded with DYD were developed via the previously reported micro-mold casting method (Zhu et al., 2014) and also presented in Table 1. Three different patches were prepared by filling the PDMS (polydimethylsiloxane) mold (Micropoint Technology, Singapore). Firstly, 1% of TCS and PVA solutions were prepared separately in 1% acetic acid solution. Then three different TCS/PVA blends of 3 ml each were prepared at the weight ratio of 7:3, 8:2 and 9:1. For incorporating DYD, 2 ml of ethanol containing 5 mg of DYD was added in 3 ml of each blend. Then PDMS molds was immersed in a pool of as-prepared solution containing polymeric blend and DYD followed by centrifugation at 5000 rpm for 4 h. Later, the filled molds were dried at room temperature for 48 h. The patch was carefully removed from the mold by applying the adhesive backing tape (Ahmad et al., 2020). The microneedle patches were prepared by using different ingredients with specifications listed in the Table 1.

3.5. Drug content determination

The microneedle patches were dissolved in methanol containing sodium lauryl sulfate (SLS). The drug was extracted by continuous stirring for 24 h. The extracted sample was analyzed on an ultraviolet (UV) spectrophotometer at 285 nm.

3.6. Fourier transform Infrared spectroscopy (FTIR) analysis

FTIR spectroscopy was carried out to investigate the chemical composition of MN-patch. The IR radiation frequencies vary among different functional groups. Therefore, Infrared spectroscopy is used for structural explanation and compound identification. The

Table 1
Composition of different polymeric blend prepared by TCS and PVA.

Formulations	1% Thiolated chitosan: 1% Poly-vinyl acetate (ml:ml)	Dydrogesterone (mg)
MN-P1	7:3	5
MN-P2	8:2	5
MN-P3	9:1	5

presence of TCS/PVA and DYD in the polymer matrix was confirmed through FTIR analysis that was performed by placing a pinch of the sample onto the crystal point of FTIR spectrophotometer Bruker alpha (Bruker, USA). The resultant spectra were analyzed between 500 and 4000 wavenumber (Nguyen et al., 2018).

3.7. Evaluation of MN-patch

3.7.1. Moisture content

The moisture content of DYD containing MN-P1, MN-P2, and MN-P3 was evaluated by weighing the patches individually and placing them in a desiccator having preheated silica gel beads for 24 h at room temperature (McCrudden et al., 2014). After the specified time, patches were again weighed and moisture content (%) was determined by using the following equation.

$$\textbf{Moisture content}(\%) = (wi - wf)/wi \times 100.$$

where,
w_i = initial weight of patch.
w_f = final weight of patch.

3.7.2. Thickness of the patch

The average thickness of all the patches MN-P1, MN-P2 and MN-P3 was determined by a digital absolute micrometer (Mitutoyo, Japan) through measurement noted at various vital areas of the patch. At first, the thickness of the glass slide was measured and microneedle patch was placed between two glass slides and measured again using micrometer. The thickness of the patch was determined by subtracting the thickness of glass slide (Naz et al., 2017).

3.7.3. Tensile strength and mechanical strength of needles

The tensile strength of the MN-P1, MN-P2 and MN-P3 was evaluated by using an auto tensile tester (Param, China) through a reported method with some modifications (Khan et al., 2000). Briefly, the patch was held between two jaws at a distance of 3 cm and was pulled by a force which was measured when patch break i.e. considered breaking force is checked by following equation.

$$\textbf{Tensile strength} = \text{Force applied to break}(\text{N})/\text{Cross sectional area of patch}(\text{cm}^2)$$

To asses the mechanical strength of the needles, compression test was performed by using universal testing machine (Testometric, UK). The developed microneedle patches were carefully palced with the needles facing downwards, on the metal platform of the probe of the machine. The probe was moved down at a speed of 0.5 mm/s for making MNs touch the platform at the force of 0.02 N for 30 s. After that the probe was moved upwards at a speed of 0.5 mm/s and the average mechanical strength was measured in "N".

3.7.4. Percentage elongation

Elongation is a basic change in structure that any object experiences under any imposed stress. In other words, when tensile strength is applied, sample deformation occurs resulting in sample elongation and stretching. Percentage elongation was evaluated when the patch broke into two pieces by applying breaking force. The initial and final lengths of the patch were determined by the auto tensile tester at breakage, (Khan et al., 2000) calculated by the following formula in equation.

$$\textbf{Percent elongation} = (l - l_0)/(l_0) \times 100.$$

where,
l_0 = initial length of the patch.
l = Final length of patch.

3.7.5. Insertion of MN-patch

The determination of microneedles skin penetration ability was carried out by a proposed parafilm M (PF) based method. The sheet of parafilm M was folded to achieve an eight-layered film (≈ 1 mm). The film was positioned on a flat surface and a microneedle patch was applied by pressing against the parafilm manually by thumb using the same force required to push the elevator button for 30 s. The parafilm M sheet was unfolded/un-rolled/opened to view the number of holes on each layer, microscopically (Larrañeta et al., 2014).

3.8. Skin irritation study

Female Balb/C mice weighing 20 ± 1 g were used for this study where the animals were acclimatized for laboratory conditions for a week. The experiment was carried out according to the approved protocol by the REC of Riphah International University with approval reference no. REC-RIPS-2021/442-A. The mice were anesthetized with 2.5 % isoflurane and their back was shaved with an electric shaver. MN-P1, MN-P2 and MN-P3 patches of DYD were applied to the mice dorsal skin by applying pressure with the thumb for 30 s. The skin was observed for signs of irritation and sensitization over a duration of 24 h (Hirobe et al., 2013).

3.9. SEM analysis

SEM was used to analyze the morphology and dimensions of the microneedle patch (Cheung and Das 2016). The samples were prepared by fixing the microneedle patch onto the glass slide using double tape. These samples were then coated with an Auto Fine Coater (JEOL, Japan) to avoid the charge effect. The needle height, base and pitch were imaged at different magnifications and microscopic images were taken by SEM microscope model (JSM 6490LA, JEOL microscope).

3.10. Optimization of microneedle patch

Based on mechanical properties and shape of microneedles on patch was selected among MN-P1, MN-P2 and MN-P3 for *in-vitro* and *ex vivo* study on basis of best mechanical properties and result of SEM indicating sharp needles.

3.11. In-vitro drug release study

The release study of DYD from microneedle patch was performed by using Franz diffusion cell. The MN-P2-patch was fixed on dialysis membrane (molecular weight cut-off 12–14 kDa) and sealed with clip and petroleum jelly. The fixed drug-loaded patch was placed between donor and receptor compartment. The MN-patch was continuously hydrated with a buffer having pH 7.4 maintained at 37 ± 1 °C. The receptor part was filled with phosphate buffer solution (pH 7.4) having 1% SLS maintained at 37 ± 1 °C using a hotplate stirrer. The 0.5 ml of the sample was withdrawn at specified time intervals (0, 0.5, 1, 2, 3, 4, 6, 8, 12, 16, 24, 36, and 48 h) and replaced with an equal volume of fresh buffer medium (Ahmad et al., 2020). Drug content was determined at 285 nm wavelength by UV–vis spectrophotometer (Shimadzu, Japan).

3.12. Ex- vivo permeation study

The skin of the Albino mice was used as a model membrane to perform an *ex vivo* permeability study by using Franz diffusion cell. The skin was shaved and de-fattened by wiping with an ethanol dipped swab. The MN-P2 patch was firmly mounted on the skin and then placed on receptor compartment (Du et al., 2019). The

receptor phase was loaded with phosphate buffer (pH 7.4) having 1% SLS preserved at 37 ± 1 °C via using a hotplate stirrer. To assess drug permeation through the skin, the sample solution of 0.5 ml was withdrawn at predetermined time points (0, 1, 2, 3, 4, 5, 6, 7, 8, 10, 12, 14, 16, 18, 20, 22, and 24 h) and restored with an equal volume of fresh medium (Abruzzo et al., 2012). The amount of drug was quantified by using UV-spectrophotometer at 285 nm wavelength. Finally, a graph was drawn between percentage cumulative drug permeated and time (Gaillard and de Boer 2000).

3.13. Skin distribution study

After 48 h of permeation study, the skin was removed from the Franz cell. The layers of skin were homogenized using a tissue homogenizer. The collected homogenate was dipped in methanol and placed on stirrer at room temperature for 24 h to completely extract DYD. The extract was analyzed using the UV-spectrophotometer method (Kathuria et al., 2016).

3.14. Histological evaluation of mice skin

The MN-P2 patch inserted into the mice' skin by pressing the patch for 30 s let it stay for 2 h. Then, a thin section was sliced and stained carefully for tissue visualization succeeded with ejection and placement of skin in a paraffin block. As-prepared sample slide was observed under a microscope (OMAX Microscope, USA) for MN-patch insertion histological changes (Lee et al., 2008).

3.15. Statistical analysis

All the experiments were carried out in triplicates and results were displayed as mean ± SD. The *in-vitro* release data were evaluated using DD solver, a free MS Excel add-in. Student's *t*-test and ANOVA was applied where required using MS Excel. A P-value < 0.05 represents statistically significant difference.

4. Results and discussion

To overcome various drug administration problems associated with oral dosage forms, pharmaceutical scientists are continuously attempting to explore the transdermal route as an alternative. For this, transdermal patches are the most preferred routes due to their exceptional benefits, including increased patient compliance, controlled drug delivery, and increased bioavailability. But still, conventional TDDS counters the major hindrance in crossing *stratum corneum* that requires additional permeation enhancers. Microneedle patches are preferred over conventional TDDS that can form a minimally invasive delivery system, painlessly pierce the *stratum corneum,* and can enhance the delivery of drug molecules to blood circulation. Therefore, microneedle patches of DYD were developed to effectively deliver to the systemic circulation and enhanced bioavailability compared to the plain drug delivered via the transdermal route (Naz et al., 2017).

4.1. Synthesis and characterization of TCS

TCS was obtained by modification of chitosan with thiol groups via EDAC coupling reaction by the formation of an amide bond between the amino group of chitosan and the carboxyl group of TGA. After lyophilization, TCS appeared as white fibrous material. The amount of thiol groups immobilized on the chitosan was 438 ± 43 µmol/g of thiolated polymer while disulfide bonds were found to be 148 ± 27 µmol/g of polymer. The disulfide bonds might have developed by the oxidation of thiol groups during the handling of the thiolated polymer.

4.2. Synthesis of the microneedle patch

Three different DYD-loaded microneedle patches (MN-P1, MN-P2, and MN-P3) were fabricated by utilizing PDMS molds and different compositions of polymeric ingredients as specified in Table 1. The MN-patches were procured having 225 needles with 200 µm base diameter and 575 µm height (as per mold manufacturer specifications). The needles obtained via a centrifugation technique showed a sharp pointed end, observed microscopically as shown in Fig. 1**.** The amount of DYD present in the patches developed from formulations MN-P1, MN-P2, and MN-P3 was found to be 1.79 ± 0.11 mg, 1.81 ± 0.09 mg, and 1.87 ± 0.24 mg respectively. A similar drug loading in all the patches might be due to the same filling capacity of the molds of the solutions containing the same amount of DYD.

4.3. ATR-FTIR analysis

ATR-FTIR analysis of chitosan displayed the characteristic peaks at 3412 cm^{-1} (hydroxyl-group), 2920 cm^{-1} (CH-bond), 1632 $cm^{-1,}$ and 1586 cm^{-1} (NH-group), 1250 cm^{-1} (OH-bond), 892 cm^{-1} (epic β-CH of cyclic pyranose rings) and 659 cm^{-1} (appeared due to amino group). Therefore, in thiolated chitosan, the amide bond is formed after the reaction of the NH_2 group of chitosan with the COOH group of TGA, which showed the peaks at 1624 cm^{-1} and 1529 cm^{-1} (amide bond) and 1250 cm^{-1} (thiol group) as shown in Fig. 2. The PVA showed absorption peaks at 1713 cm^{-1} (C = O group), 1375 $cm^{-1,}$ and 1141 cm^{-1} (C-O group). The FTIR spectrum of DYD showed three carbonyl groups at wavenumbers 1695 cm^{-1} and 1657 cm^{-1}, whereas the band for hydroxyl groups appeared at wavenumbers 3256 cm^{-1} and the double band is located at 875 cm^{-1}.The FTIR spectrum of the MN-P3 indicates the presence of distinct peaks of DYD, amide bond of thiolated chitosan.

4.4. Evaluation of microneedle patch

4.4.1. Moisture content

The presence of moisture affects the various physical properties of the patch i.e. flexibility, brittleness, and fragility (Singh et al., 2009). The moisture content of all microneedle patches is presented in Fig. 3**.** The % moisture content of MN-P1, MN-P2, and MN-P3 was found to be 3.2 ± 0.44 %, 3.5 ± 0.32 % and 3.0 ± 0.2 % respectively. An increase in moisture content of MN-P2 as compared to MN-P1 might be due to the increase in the number of thiol groups that can develop disulfide bonds resulting in the crosslinking of the matrix thus entrapping increased moisture. However, the moisture content was lowest when the concentration of thiolated polymers was maximum which might be due to the increased crosslinking of the thiol groups by disulfide bond formation might have resulted in the rigid structure with reduced ability to hold moisture.The moisture content also affected the the average thickness of the patches as the the patch with highest moisture content was having the highest thickness Fig. 4

4.4.2. Tensile, mechanical strength and percentage elongation

The tensile strength plays a significant role in the complete removal of dried MN-patch from the mold and for application on the skin. MN-P1. MN-P2 and MN-P3 were analyzed for tensile test and results are presented in Fig. 5. The formulation of MN-P2 showed the best tensile strength of 0.046 ± 0.01 N/cm^2. The MN-P1 and MN-P3 showed 0.042 ± 0.01 and 0.046 ± 0.02 N/cm^2 respectively.

Mechanical strength was found to be 0.47 ± 0.12, 1.24 ± 0.41 and 0.97 ± 0.21 N for the patches MN-P1, MN-P2 and MN-P3 respectively. A breaking force greater than 0.24 N is considered suitable for the insertion into the skin however the greatest break-

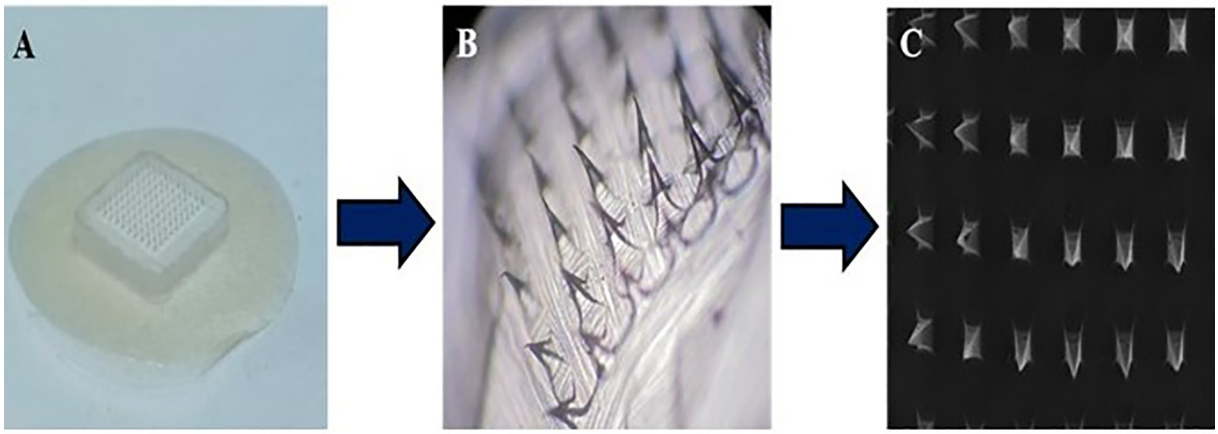

Fig. 1. A) Image of developed MN-P2 patch, B) Microscopic view of MN-P2 and C) SEM images of MN-P2 showcasing sharp pointed needles.

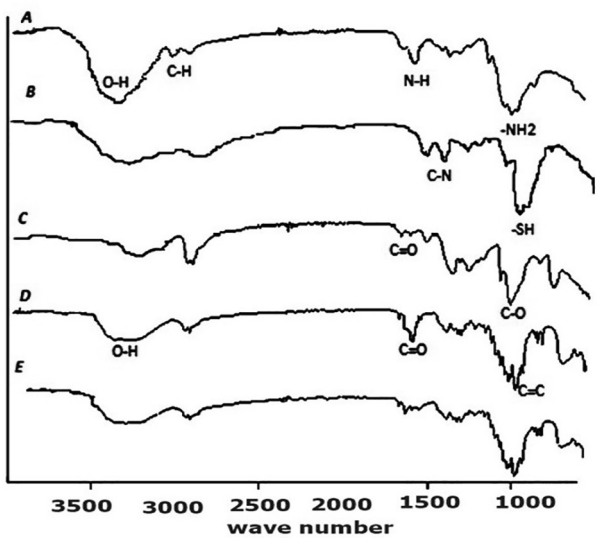

Fig. 2. FTIR spectrum of A = polymer chitosan, B = thiolated chitosan, C = Poly-vinyl acetate, D = DYD(drug), E = sample of DYD-loaded TCS-PVA showing characteristic peaks at different wave number (cm^{-1}).

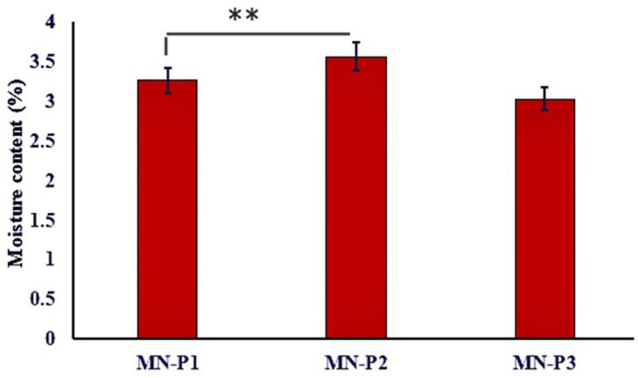

Fig. 3. Graphical representation of moisture content (%) of MN-Patches. The results are expressed as mean ± S.D, n = 3.

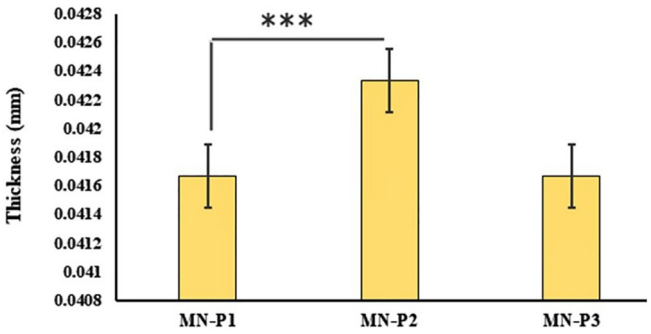

Fig. 4. The results of average thickness of MN-Patches are expressed as mean ± S.D, n = 3.

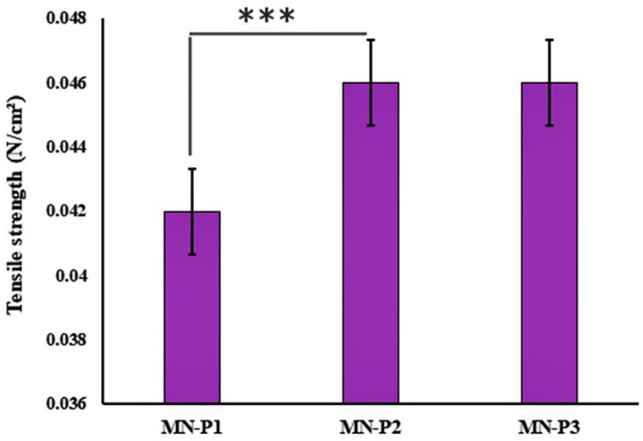

Fig. 5. Results of tensile strength of prepared MN-patches. The results are expressed as mean ± S.D, n = 3.

ing force in case of MN-P2 may be attributed to the crosslinking of the thiolated polymer. The increased mechanical strength of MN-P3 may be related to cross-linking of polymeric chains caused by the formation of disulfide bonds and increased moisture content that might have provided the flexibility and thus resistance to brittleness. The patch MN-P3, although containing the highest amount of thiolated polymer and thus increased crosslinking, showed lower strength due to its hard structure and less flexibility, thus showing brittleness at the lower force compared to MN-P2 with highest moisture content providing the flexibility to the matrix. Similarly, the maximum elongation shown by MN-P2 was 34.06 ± 1.18% (Fig. 6) compare to 32.83 ± 1.68% and 31.7 ± 0.41% of MN-p1 and MN-P3 respectively.

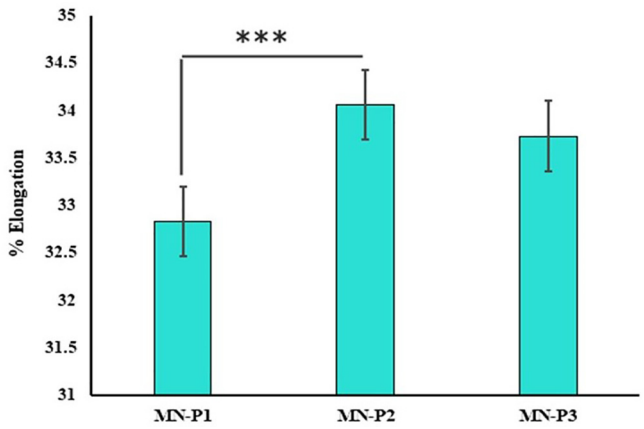

Fig. 6. Percentage elongation of prepared MN-patches with mean ± S.D, *n* = 3.

4.4.3. Insertion of MNP/penetration evaluation of MN-patch

The design of microneedles was governed by factors that include polymeric materials and methods opted for fabrication, which was essential for microneedles to have the adequate mechanical strength to be inserted into the skin without failure. The penetration of microneedles in the skin was confirmed by skin penetration studies using the parafilm method. The results explained that needles of MN-P2, successfully pierced the four layers of parafilm as 225 holes (no. of needles in each patch) were observed microscopically as shown in Fig. 7. The microscopic examination of the patch presents no deformation of needles and shows that most needles remain intact to base and retained their endpoints. The lower concentration of thiolated polymer in MN-P1 produced less disulfide crosslinked density thus indicating lower mechanical strength which failed to withhold the pressure. Similarly, at higher concentrations, the needles were more fragile indicating brittleness due to the decreased flexibility owing to reduced moisture contents.

4.5. Irritation study

The irritation study was performed to observe for the signs of erythema or any abnormal interaction with the skin. The results are shown in Table 2 indicating no sign of irritation or redness on the skin after application of microneedle patches MN-P1, MN-P2 and MN-P3.

4.5.1. SEM analysis

The morphology of the prepared microneedle patches was analyzed through scanning electron microscopy as presented in Fig. 8**.** The SEM images of MN-P2 indicate the pyramid shape of intact needles and sharp pointed ends, with a length of 535 µm. The slight decrease in dimensions may be due to solvent evaporation during drying resulting in the solidification and contraction of a matrix.

4.5.2. Optimization of microneedle patch

The optimization of the microneedle patches was done based on tensile strength, percentage elongation, and sharpness of the needles as all these factors influence the proper insertion of the patches into the skin. Based on the results discussed above the MN-P2 was most suitable having maximum tensile strength, % age elongation and sharpness of the needles. MN-P2 was further used for further studies.

4.6. In-vitro drug release study

The *in-vitro* release study was performed using Franz-diffusion cell using dialysis membrane and the results are presented in Fig. 9. The DYD release study of MN-Patch showed a sustained release of DYD over a time of 48 h with a maximum release of 81.45 ± 2.768 %. These results are consisted with other reports on the microneedle based transdermal delivery system reporting a 65 %, 80 % and 82.5 % of drug release in 48 hrs. in comparison to the MN-P2 the suspension of pure drug exhibited 96.7 ± 1.75

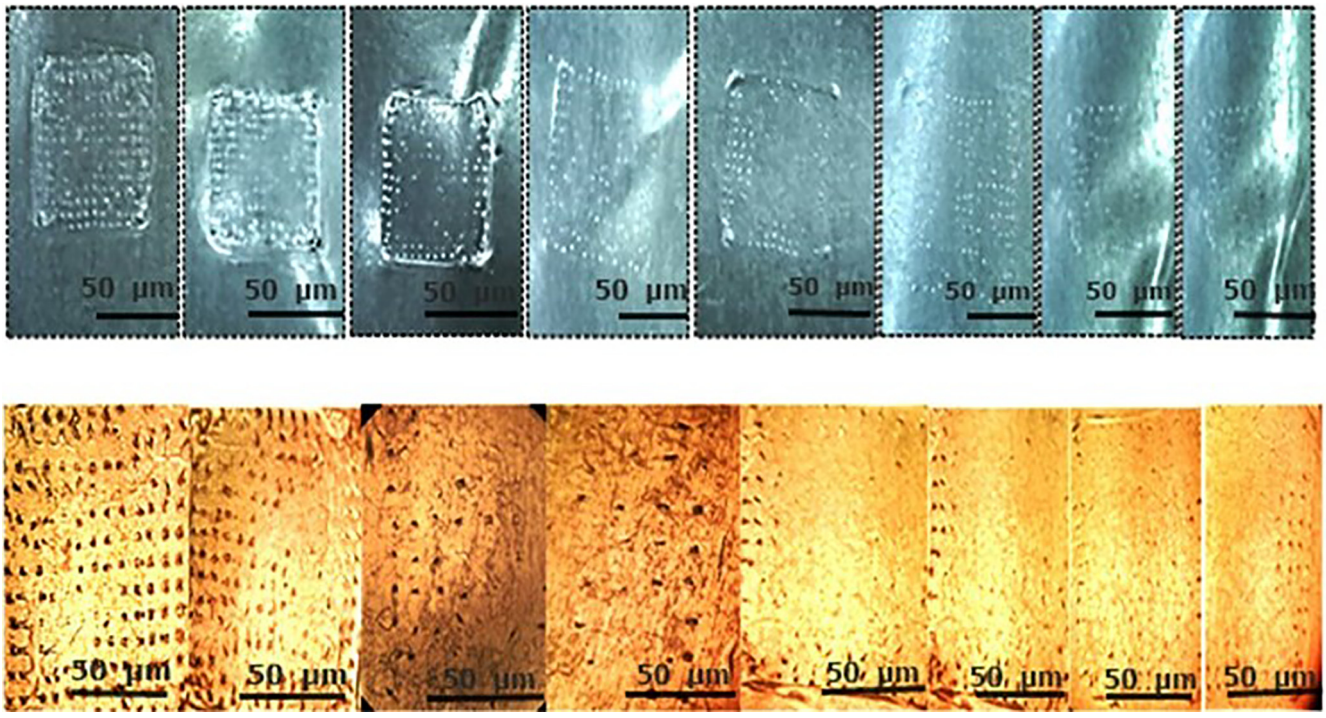

Fig. 7. Skin penetration study is performed by modified parafilm M method. Firstly, an 8 folded PF-M attached to micro needle patch (A), and a sequential layer of PF-M, view of PF-M after insertion of MN-patch for 30 s, post microscopic view of an inserted layer (B).

Table 2
Observations of irritation study on mice skin.

Sr #	Patch	Number of samples	Irritation observed
1	MN-P1	3	No
2	MN-P2	3	No
3	MN-P3	3	No

% in 12 h. The DYD is recognized as the drug with very poor dissolution profile that might be the reason for its very slow dissolution. The drug release through biodegradable polymer carrier involves passive diffusion, controlled swelling and matrix degradation (Stewart et al., 2018). The purpose of using thiolated polymer was to design disulfide crosslinked matrix that can retard the release of DYD via slow passive diffusion, controlled swelling and biodegradability due to disulfide exchange with cellular glutathione. In case of microneedle patches, although the needle easily crossed the dialysis membrane barrier, DYD release was much slower compared to pure drug due to the disulfide crosslinked matrix of the patches that hindered the release of DYD.

The drug release data was subjected to kinetic analysis via different mathematical models as shown in Table 3, i.e. zero-order, first-order, Higuchi and Korsmeyer-Peppas. The first order kinetic analysis indicated R^2 of 0.9293 as compared to 0.6341 in case of zero order kinetics indicating a concentration dependent release of DYD via passive diffusion. While processing release data in Korsmeyer-peppas model the value of n was found to be 0.482 indicating non-fickian diffusion that might be due to the slow degradation of the microneedles. The microscopic images of the patches at different time intervals after dissolution clearly indicate the changed morphology of the needles as shown in the Fig. 10.

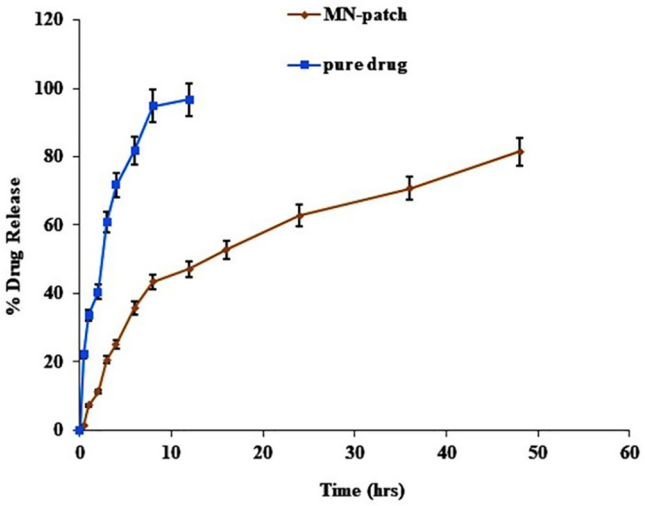

Fig. 9. The results of the *in-vitro* study of DYD from MN-patch and pure drug evaluated by Franz diffusion cell over a period of 48 h. The results of triplicate are shown as mean ± S.D, *n* = 3.

Table 3
Kinetic assessment of *in-vitro* dissolution study by various kinetic model equations.

Kinetic model	MN Patch	
	Slope	**R^2**
Zero-order	k_0 = 2.152	0.6341
First-order	k_1 = 0.049	0.9293
Higuchi	k_H = 12.409	0.9676
Korsmeyer-Peppas	k_{KP} = 13.134 n = 0.482	0.9683

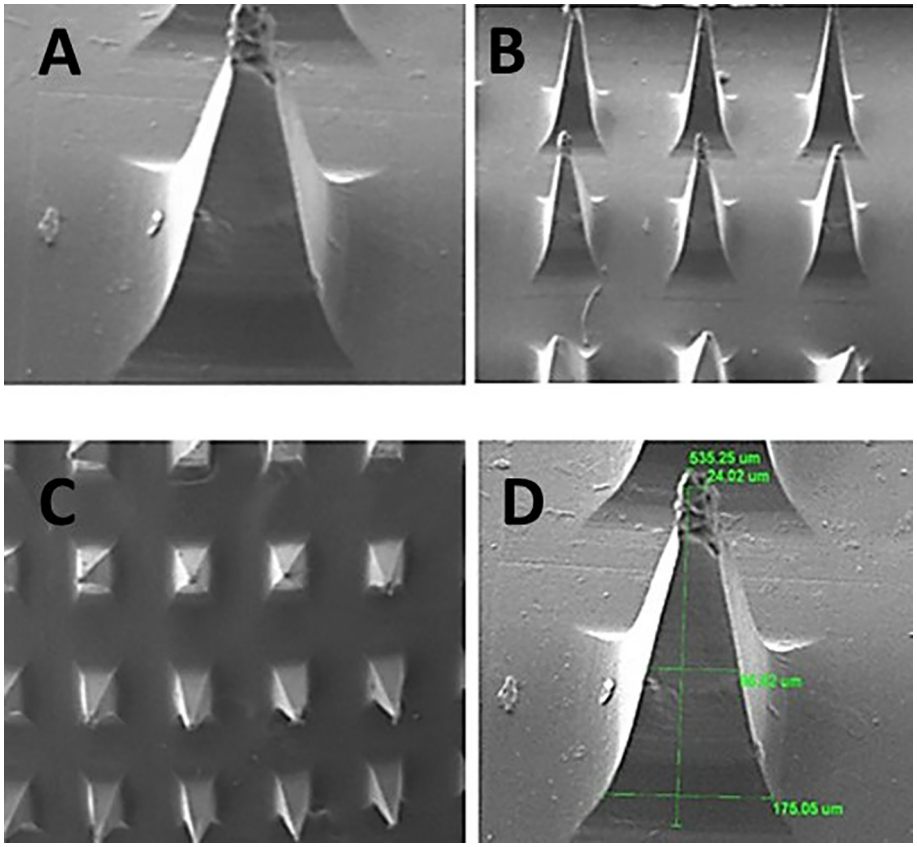

Fig. 8. Scanning electron microscopy (SEM) micrograph images of MN-patch at different magnification powers (A) a single needle showing pyramidal shape at higher resolution (B), (C) and (D) an MN-patch array showing pointed needles at lower resolutions.

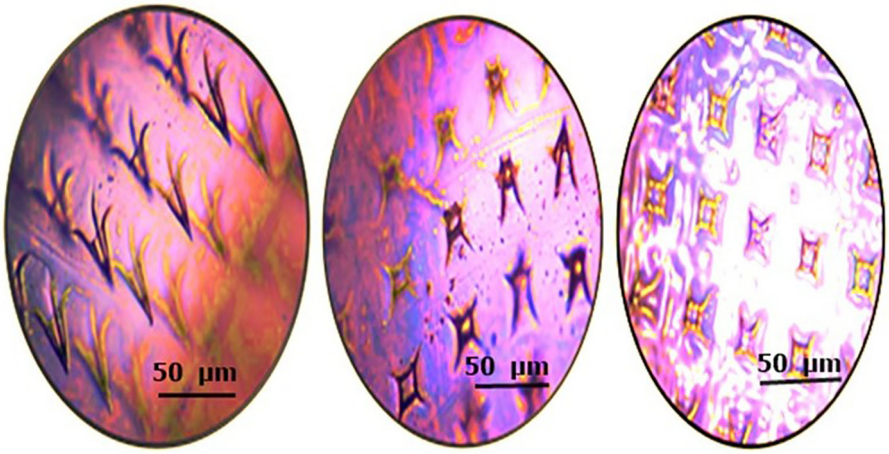

Fig. 10. Microscopic view of MN-patch at different time intervals (A) at 0 h, (B) at 24 h (C) 48 h, representing the clear changes in the morphology of micro-needles due to degradation and dissolution.

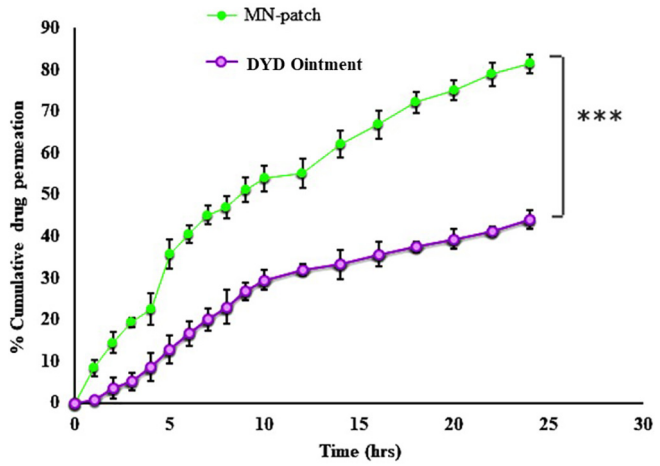

Fig. 11. The results of the *ex-vivo* skin permeation of DYD from MN-patch and Pure drug evaluated by Franz diffusion cell over a period of 24 h. The results of triplicates are shown with mean ± S.D, $n = 3$.

4.7. Ex-vivo permeation study

The *ex-vivo* permeation was evaluated in terms of amount of DYD transported across mice skin via franz-diffusion cell by using MN-P2 and DYD ointment prepared in the lab for the purpose of holding the DYD at the contact area and results are presented in Fig. 11.

The percentage of DYD permeated with MN-P2 was found to be 81.46 ± 2.25 % compared to 43.96 ± 2.27 % of drug permeation in case of DYD ointment indicating a significant difference in the permeation of DYD ($P < 0.05$). The transport across the stratum corneum was restricted due to high molecular weight. The 1.85-fold enhanced permeation due MN-P2 is facilitated by the microspores formed by microneedles insertion, which directly aided the transport of drug through deeper skin layers (Salem et al., 2019).

4.8. Skin distribution study

The amount of DYD present in the skin was determined by extracting the drug from the tissue. The results indicated the presence of 15.18 ± 1.22 % and 8.95 ± 2.51 % of DYD in the skin tissues in case of MN-P2 and DYD ointment respectively.

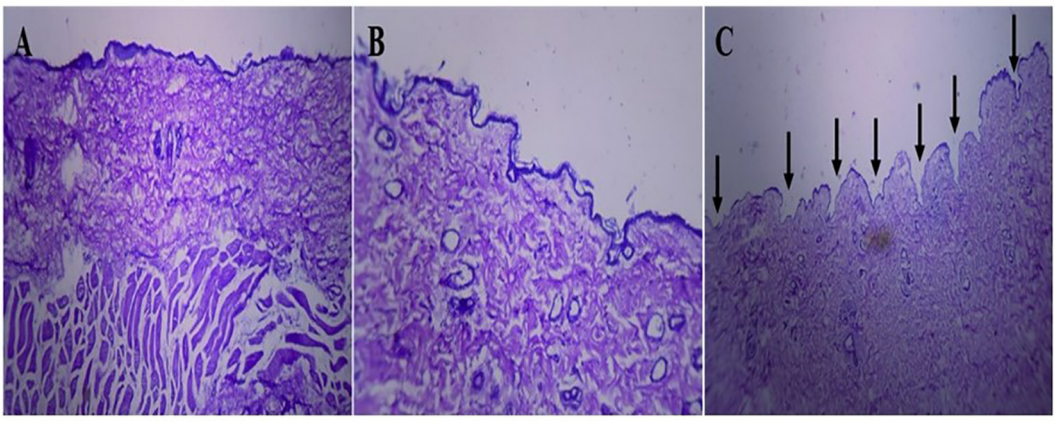

Fig. 12. A microscopic histological evaluation showing (A) normal skin (B) skin after 2 min of microneedle patch applied (C) skin after application of 1 h of a microneedle patch.

4.9. Histological evaluation of mice skin

Histological examination of mice skin with microneedle patch showed penetration depth into the superficial dermis via a stratum corneum**.** A cross-sectional image of skin at a side of microneedle patch penetration showed in Fig. 12**.** The histological study revealed, successful insertion of DYD microneedles bypassing the stratum corneum, epidermal layer and superficial dermis. Thus, penetration to the epidermis layer will maximize the transdermal drug delivery, which was reported as the major advantage of microneedles patch (Gupta et al., 2011).

5. Conclusions

The present study was aimed to prepare microneedle patch (MN-P) as an alternative route for the administration of DYD. The MN-patch was fabricated by using PDMS mould with different ratios of TCS and PVA by micro-molding method. The MN-P presented better results in scanning electron microscopy, mechanical properties, drug release and physiochemical properties. The microneedles successfully prorated the skin to create uniform micro channels to facilitate the transport across skin. The insertion of microneedles resulted in prolonged delivery system of DYD against the skin. The TCS-PVA based microneedle array has markedly change the release and delivery profile of DYD *in-vitro* and *ex-vivo* at physiological pH, compared to pure drug and DYD ointment. Thus, it can be concluded that the microneedle patch based system can be a promising delivery system for the effective delivery of DYD.

Funding

This research received no external funding.

Institutional Review Board Statement

Not applicable.

Informed Consent Statement

Not applicable.

Declaration of Competing Interest

The authors declare that they have no known competing financial interests or personal relationships that could have appeared to influence the work reported in this paper.

Acknowledgments

The authors would like to extend their sincere appreciation to the researchers supporting the Project No. RSP2023R457, King Saudi University Riyadh, Saudi Arabia. The Authors are also thankful and would like to extend their acknowledgement to Al Ain University.

References

Abruzzo, A., Bigucci, F., Cerchiara, T., et al., 2012. Mucoadhesive chitosan/gelatin films for buccal delivery of propranolol hydrochloride. Carbohydr. Polym. 87, 581–588.

Ahmad, Z., Khan, M.I., Siddique, M.I., et al., 2020. Fabrication and characterization of thiolated chitosan microneedle patch for transdermal delivery of tacrolimus. Aaps Pharmscitech. 21, 1–12.

Amer, R.I., Yassin, G.E., Mohamed, R.A., et al., 2021. Pharmaceutical and pharmacological evaluation of the effect of nano-formulated spironolactone and progesterone on inflammation and hormonal levels for managing hirsutism experimentally induced in rats. AAPS PharmSciTech. 22, 1–11.

Arshad, R., Sohail, M.F., Sarwar, H.S., et al., 2019. ZnO-NPs embedded biodegradable thiolated bandage for postoperative surgical site infection: In vitro and in vivo evaluation. PLoS One. 14, e0217079.

Bernkop-Schnürch, A., Schwarz, V., Steininger, S., 1999. Polymers with thiol groups: a new generation of mucoadhesive polymers? Pharm. Res. 16, 876–881.

Cheung, K., Das, D.B., 2016. Microneedles for drug delivery: trends and progress. Drug Deliv. 23, 2338–2354.

Du, H., Liu, P., Zhu, J., et al., 2019. Hyaluronic acid-based dissolving microneedle patch loaded with methotrexate for improved treatment of psoriasis. ACS Appl. Mater. Interfaces 11, 43588–43598.

Elahpour, N., Pahlevanzadeh, F., Kharaziha, M., et al., 2021. 3D printed microneedles for transdermal drug delivery: a brief review of two decades. Int. J. Pharm. 597, 120301.

Gaillard, P.J., de Boer, A.G., 2000. Relationship between permeability status of the blood–brain barrier and in vitro permeability coefficient of a drug. Eur. J. Pharm. Sci. 12, 95–102.

Gupta, J., Gill, H.S., Andrews, S.N., et al., 2011. Kinetics of skin resealing after insertion of microneedles in human subjects. J. Control. Release 154, 148–155.

Hirobe, S., Azukizawa, H., Matsuo, K., et al., 2013. Development and clinical study of a self-dissolving microneedle patch for transcutaneous immunization device. Pharm. Res. 30, 2664–2674.

Iqbal, J., Shahnaz, G., Perera, G., et al., 2012. Thiolated chitosan: development and in vivo evaluation of an oral delivery system for leuprolide. Eur. J. Pharm. Biopharm. 80, 95–102.

Jung, J.H., Jin, S.G., 2021. Microneedle for transdermal drug delivery: current trends and fabrication. J. Pharm. Investig. 51, 503–517.

Kathuria, H., Li, H., Pan, J., et al., 2016. Large size microneedle patch to deliver lidocaine through skin. Pharm. Res. 33, 2653–2667.

Khan, T.A., Peh, K.K., Ch'ng, H.S., 2000. Mechanical, bioadhesive strength and biological evaluations of chitosan films for wound dressing. J. Pharm. Pharm. Sci. 3, 303–311.

Larrañeta, E., Moore, J., Vicente-Pérez, E.M., et al., 2014. A proposed model membrane and test method for microneedle insertion studies. Int. J. Pharm. 472, 65–73.

Lee, J.W., Park, J.-H., Prausnitz, M.R., 2008. Dissolving microneedles for transdermal drug delivery. Biomaterials 29, 2113–2124.

McCrudden, M.T., Alkilani, A.Z., McCrudden, C.M., et al., 2014. Design and physicochemical characterisation of novel dissolving polymeric microneedle arrays for transdermal delivery of high dose, low molecular weight drugs. J. Control. Release 180, 71–80.

Naz, K., Shahnaz, G., Ahmed, N., et al., 2017. Formulation and in vitro characterization of thiolated buccoadhesive film of fluconazole. Aaps Pharmscitech. 18, 1043–1055.

Nguyen, H.X., Bozorg, B.D., Kim, Y., et al., 2018. Poly (vinyl alcohol) microneedles: fabrication, characterization, and application for transdermal drug delivery of doxorubicin. Eur. J. Pharm. Biopharm. 129, 88–103.

Parın, F.N., Aydemir, Ç.İ., Taner, G., et al., 2022. Co-electrospun-electrosprayed PVA/folic acid nanofibers for transdermal drug delivery: Preparation, characterization, and in vitro cytocompatibility. J. Ind. Text. 51, 1323S–1347S.

Sabbagh, F., Kim, B.S., 2022. Recent advances in polymeric transdermal drug delivery systems. J. Control. Release 341, 132–146.

Sabo, S., Waters, L.J., 2021. Poly (dimethylsiloxane): a sustainable human skin alternative for transdermal drug delivery prediction. J. Pharm. Sci. 110, 1018–1024.

Salem, H.F., Kharshoum, R.M., Abou-Taleb, H.A., et al., 2019. Progesterone-loaded nanosized transethosomes for vaginal permeation enhancement: formulation, statistical optimization, and clinical evaluation in anovulatory polycystic ovary syndrome. J. Liposome Res. 29, 183–194.

Saremi, S., Atyabi, F., Akhlaghi, S.P., et al., 2011. Thiolated chitosan nanoparticles for enhancing oral absorption of docetaxel: preparation, in vitro and ex vivo evaluation. Int. J. Nanomed. 6, 119.

Sharma, G., Alle, M., Chakraborty, C., et al., 2021. Strategies for transdermal drug delivery against bone disorders: a preclinical and clinical update. J. Control. Release 336, 375–395.

Singh, T.R.R., McCarron, P.A., Woolfson, A.D., et al., 2009. Physicochemical characterization of poly (ethylene glycol) plasticized poly (methyl vinyl ether-co-maleic acid) films. J. Appl. Polym. Sci. 112, 2792–2799.

Stewart, S.A., Domínguez-Robles, J., Donnelly, R.F., et al., 2018. Implantable polymeric drug delivery devices: Classification, manufacture, materials, and clinical applications. Polymers 10, 1379.

Zhu, Z., Luo, H., Lu, W., et al., 2014. Rapidly dissolvable microneedle patches for transdermal delivery of exenatide. Pharm. Res. 31, 3348–3360.